J. Fluid Mech. (1990), vol. 216, pp. 585–611
Printed in Great Britain

On the instabilities of supersonic mixing layers: a high-Mach-number asymptotic theory

By THOMAS F. BALSA[1] AND M. E. GOLDSTEIN[2]

[1] Aerospace and Mechanical Engineering Department, University of Arizona, Tucson, AZ 85721, USA

[2] National Aeronautics and Space Administration, Lewis Research Center, Cleveland, OH 44135, USA

(Received 17 February 1989 and in revised form 18 December 1989)

The stability of a family of tanh mixing layers is studied at large Mach numbers using perturbation methods. It is found that the eigenfunction develops a multilayered structure, and the eigenvalue is obtained by solving a simplified version of the Rayleigh equation (with homogeneous boundary conditions) in one of these layers which lies in either of the *external* streams. Our analysis leads to a simple hypersonic similarity law which explains how spatial and temporal phase speeds and growth rates scale with Mach number and temperature ratio. Comparisons are made with numerical results, and it is found that this similarity law provides a good qualitative guide for the behaviour of the instability at high Mach numbers.

In addition to this asymptotic theory, some fully numerical results are also presented (with no limitation on the Mach number) in order to explain the origin of the hypersonic modes (through mode splitting) and to discuss the role of oblique modes over a very wide range of Mach number and temperature ratio.

1. Introduction

There has recently been a resurgence of interest in the stability characteristics of supersonic mixing layers (Papamoschou 1986; Jackson & Grosch 1988; Tam & Hu 1988). The primary motivation seems to come from its potential application to the design of hypersonic propulsion systems (Kumar, Bushnell & Hussaini 1987).

This paper is concerned with the inviscid instabilities of a compressible mixing layer at the interfacial region between two coflowing uniform streams when a Mach number, m_1, based on the velocity difference of these streams, is much larger than unity.

The basic formulation of the compressible shear flow stability problem (in both free and wall-bounded shear flows) is given by Lees & Lin (1946). Miles (1958) used the vortex sheet model to study the stability of free shear layers and concluded that the flow becomes neutrally stable above a certain supersonic Mach number which depends on the temperature ratio across the vortex sheet. Subsequent analyses by Blumen (1970), Blumen, Drazin & Billings (1975), and Lessen, Fox & Zien (1965), who considered finite-thickness mixing layers, but only for isothermal flows, showed that the actual flow merely becomes less unstable to temporally growing disturbances at high Mach numbers. Gropengiesser (1969), and later Jackson & Grosch (1988), considered the non-isothermal case for the more realistic, spatially growing modes.

The high-Mach-number stability characteristics of these flows appear to be quite complex and, in this paper, we attempt to sort these out by developing a high-Mach-number asymptotic solution to the compressible Rayleigh equation for a general non-isothermal free shear flow. Cowley & Hall (1990) recently obtained such a solution for a wall-bounded flow, but the structure of our solution is quite different from theirs. Like the Cowley & Hall (1990) result, our eigensolutions exhibit a multilayered structure, but in our case, there are (usually) five distinct layers rather than just two as in the Cowley & Hall (1990) analysis.

We base our asymptotic scaling on the numerical work of Jackson & Grosch (1988), which shows that, at high Mach numbers, there are two distinct instability modes whose neutral wavenumbers do not decrease and whose (real) phase speeds approach the velocities of the external streams as the Mach number becomes large. For definiteness, we restrict the discussion and analysis to the so-called 'slow mode' whose (real) phase velocity approaches that of the low-speed stream, but the result is then extended to the 'fast mode' by symmetry arguments. Under certain conditions, Jackson & Grosch also find a third mode whose instability characteristics are very unusual. This is discussed more fully in §2; however, we emphasize that our work does *not* focus on this third mode.

Benny & Bergeron (1969) were the first to consider shear-layer vorticity waves with phase velocities approaching that of the free stream. Bodonyi, Smith & Gajjar (1983) further extended these ideas in a different setting.

We find that aerodynamic or viscous heating of the base flow causes the coefficient of one of the terms in Rayleigh's equation to become very large in the limit as the Mach number, m_1, goes to infinity (the coefficient behaves as $O(m_1^4)$) and that the equation can be solved by the WKBJ method in the main part of the shear layer. However, this solution does not satisfy the appropriate boundary conditions in the external streams, and two additional 'edge layers' (essentially in the two external streams) have to be introduced. The structure of the *high-speed* edge-layer solution depends on the propagation angle, θ, of the wave. This solution is again of the WKBJ type when $\cos\theta$ is bounded away from zero (i.e. $m_1\cos\theta \gg 1$). The main shear-layer WKBJ solution then contains a turning point at the sonic point (where the wave is moving transonically relative to the base flow). This solution is oscillatory (i.e. of 'Mach wave' form) on the high-speed side of the turning point but grows exponentially towards the low-speed stream (i.e. is of 'incompressible' form).

The turning point moves into the high-speed edge layer when $\cos\theta \approx 0$ (i.e. $m_1\cos\theta = O(1)$) in the limit as $m_1 \to \infty$. The solution for this case (which satisfies the appropriate free-stream boundary condition) is given by a confluent hypergeometric function. This solution then matches onto the exponentially growing WKBJ solution in the main shear layer. The latter solution, therefore, becomes exponentially large as it approaches the low-speed stream in both cases (i.e. for all θ, $-\frac{1}{2}\pi \leqslant \theta \leqslant \frac{1}{2}\pi$) and has to be brought to zero through the low-speed edge layer.

The flow in this edge layer is governed by a 'reduced' (i.e. simplified) Rayleigh equation that involves the wavenumber and the, as yet, unknown complex phase-speed perturbation (i.e. the scaled difference between the actual complex phase speed and the low-speed stream velocity) as parameters. The solution to this equation must exhibit exponential *decay* towards the main shear layer in order to match onto the exponentially *growing* WKBJ solution in this region, and must also go to zero in the low-speed stream in order to satisfy the appropriate boundary conditions there. This leads to a homogeneous boundary-value problem which determines the complex

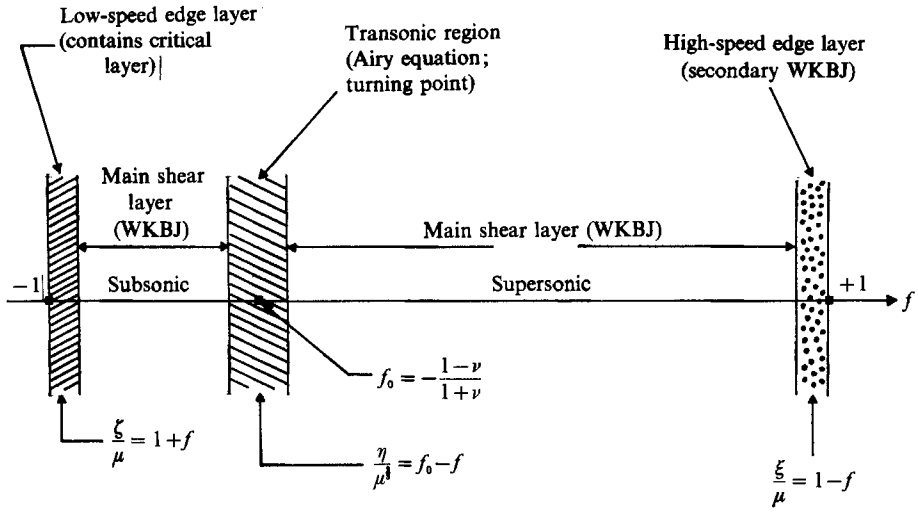

FIGURE 1. The various regions of the instability mode at large Mach numbers. $\mu = (\frac{1}{2}m_1)^2$, $f_0 \neq 1$.

phase-speed perturbation as its eigenvalue. These various regions are shown in figure 1.

The eigenvalue problem is, therefore, completely decoupled from the flow (i.e. the eigenfunction structure) in the rest of the shear layer. It is possible to derive a hypersonic similarity rule from these considerations. This rule provides a simple scaling of the instability (i.e. growth rate and (real) phase speeds) as a function of Mach number, temperature ratio, and wavenumber or frequency.

Like the original Rayleigh equation, the reduced Rayleigh equation has a regular singular point – indicating that the critical layer has moved into the low-speed edge layer. However, the eigenfunctions themselves are (surprisingly) non-singular there because the critical layer coincides with the generalized mean flow inflection point, which also moves into the low-speed layer as $m_1 \to \infty$. It is worth noting that these inflectional asymptotic modes are the continuations of non-inflectional finite-Mach-number modes, at least to the order of accuracy to which our analysis is carried out.

The plan of the paper is as follows. The problem is formulated in §2, and the WKBJ solution for the main shear layer is constructed in §3. Section 4 is concerned with the high-speed edge layer, and in §5, we consider the flow in the transonic layer for the case where this layer is distinct from the upper-edge layer (i.e. $\cos\theta \neq 0$). The low-speed edge layer is treated in §6, and the eigenvalue problem for the complex phase speed is formulated there: i.e. we derive a differential equation containing a complex parameter (the eigenvalue) along with appropriate homogeneous boundary conditions. We solve this problem numerically and thereby determine the eigenvalue using a standard finite-difference procedure. This leads to a hypersonic similarity law, which is discussed in §7 along with the numerical computations. Other numerical results (for the full Rayleigh problem) are used to describe the splitting of the original low-Mach-number instability mode into two distinct modes as the Mach number increases and to explain how these two modes are connected with the neutral modes in Miles' (1958) vortex-sheet analysis.

2. Formulation of problem

In order to investigate the linear stability of a compressible mixing layer, we invoke the usual assumptions (i.e. parallel base flow, inviscid disturbances, etc.) of classical stability theory (Betchov & Criminale 1967; Drazin & Reid 1981), and write the Rayleigh equation for the modal pressure amplitude, $p = p(y)$, as

$$\frac{\mathrm{d}^2 p}{\mathrm{d}y^2} - 2\frac{\dfrac{\mathrm{d}f}{\mathrm{d}y}}{f-\hat{c}}\frac{\mathrm{d}p}{\mathrm{d}y} + Qp = 0, \tag{1a}$$

where

$$Q = -\kappa^2 T^2[1-(\tfrac{1}{2}m_1)^2\cos^2\theta(f-\hat{c})^2/T]. \tag{1b}$$

The above form of the Rayleigh equation is slightly different from that derived by Betchov & Criminale (1967, p. 177) because in our equation y is a modified cross-space coordinate (to be defined more precisely below); our form of the Rayleigh equation is also used by Gropengiesser (1969) and by Jackson & Grosch (1988). The actual pressure perturbations in the shear layer are expressed as

$$p(y)\exp[\mathrm{i}(k(x-ct)+lz)]+\mathrm{cc}, \tag{1c}$$

where (x, z) are the streamwise and spanwise coordinates and time is denoted by t. In (1c), (k, l) are the streamwise and spanwise wavenumbers (which may be complex), c is the (complex) phase speed (or the eigenvalue) of the mode and $\mathrm{i} = (-1)^{\frac{1}{2}}$. The symbol cc denotes the complex conjugate of the term it follows in an expression.

The Rayleigh equation, (1a), is written in terms of a 'normalized' base flow velocity, $f = f(y)$, and a 'normalized' eigenvalue, $\hat{c}$, which are related to the corresponding physical variables by

$$U = U_{\mathrm{m}} + \tfrac{1}{2}\Delta U f, \tag{2a}$$

and

$$c = U_{\mathrm{m}} + \tfrac{1}{2}\Delta U \hat{c}, \tag{2b}$$

where U_{m} and ΔU denote the average speed of and the velocity difference across the mixing layer respectively; $U_{\mathrm{m}} = \frac{1}{2}(U_1+U_2)$, $\Delta U = U_1 - U_2 > 0$. The velocities of the external streams at $y = \pm\infty$ are given by $U_{1,2} = \text{const.}$ and the velocity of the unperturbed base flow is $[U(y), 0, 0]$. We introduce these 'normalized' or canonical quantities f and $\hat{c}$ because the eigenvalue $\hat{c}$ – as a function of the wavenumbers k and l – will then be independent of the external stream velocities, U_1 and U_2. The similarity parameters associated with this problem are discussed at the end of this section; for a picture of the mixing layer see figure 2.

The remaining variables in (1b) are the total wavenumber

$$\kappa = (k^2+l^2)^{\frac{1}{2}} \tag{3a}$$

(whose real part is taken to be non-negative), the obliqueness angle, θ, defined by

$$k = \kappa\cos\theta \tag{3b}$$

and

$$l = \kappa\sin\theta, \tag{3c}$$

the unperturbed (non-dimensional) temperature, T, of the mixing layer, which is normalized so that $T = 1$, T_2 at $y = \pm\infty$, respectively, where y is related to the *physical* cross-stream variable, Y, through the Howarth–Dorodnitsyn transformation

$$Y = \int_0^y T\,\mathrm{d}y, \tag{3d}$$

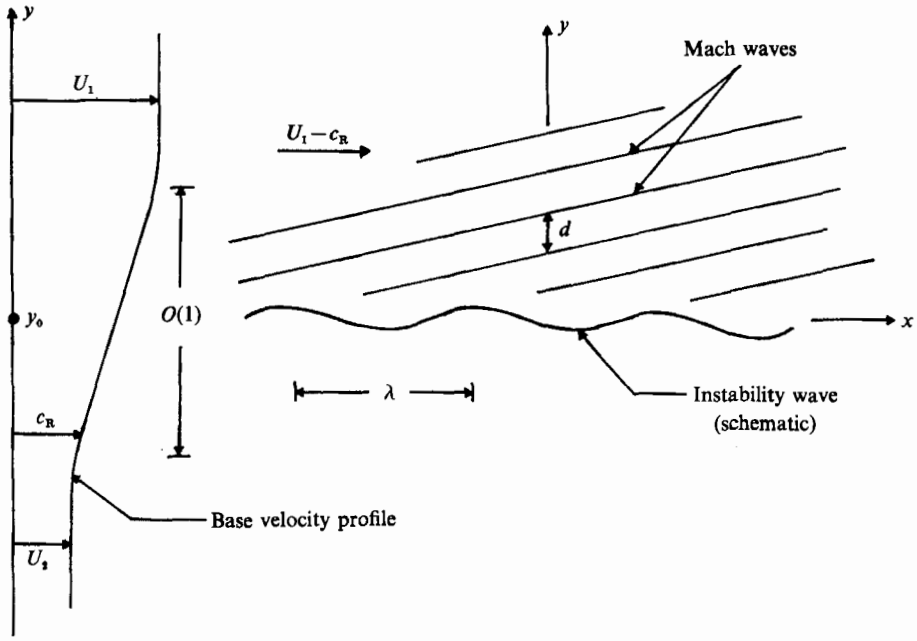

FIGURE 2. Schematic representation of the flow field. $y_0 = \tanh^{-1} f_0$; f_0 = WKBJ turning point.

and, finally, m_1 is the Mach number based on the velocity difference across the mixing layer and the unperturbed speed of sound at $y = +\infty$, i.e.

$$m_1 = \frac{\Delta U}{a_1}, \quad a_1 = \text{unperturbed sound speed at } y = +\infty. \tag{4}$$

We use a lower case m to denote this Mach number and reserve the letter M for a more conventional Mach number, say $M_1 = U_1/a_1$ as is customary in aerodynamics. Note that, by symmetry, there is another Mach number which is on equal footing with (4), namely, $m_2 = \Delta U/a_2$ but this parameter is eliminated in favour of the temperature ratio $T_2 = (m_1/m_2)^2$. The unperturbed sound speed at $y = -\infty$ is given by a_2. Our normalization clearly shows that the important Mach number of the problem is the one based on the velocity difference across the mixing layer.

Finally, we note that the angle θ denotes the direction of propagation (with respect to the x-axis) of the phase fronts of the instability wave when the wavenumbers are real (temporal stability) or, the direction along which the instability wave exhibits maximum spatial growth, when the wavenumbers are complex (spatial stability).

In this paper the mean velocity and temperature profiles, f and T, will be specified as follows: we suppose that the Prandtl number is unity and that the fluid is a thermally and calorically perfect gas so that T is given by Crocco's equation

$$T = 1 + \tfrac{1}{2}(\gamma - 1)(\tfrac{1}{2}m_1)^2(1 - f^2) - \tfrac{1}{2}(1 - T_2)(1 - f), \tag{5a}$$

where $\gamma = \text{const.}$ is the isentropic exponent. The assumptions under which the Crocco equation is valid are discussed in Moore (1964); both the Crocco equation and the Howarth–Dorodnitsyn transformation are familiar entities in compressible boundary-layer theory (Schlichting 1968, pp. 315, 324) and in hypersonic flow theory (Hayes & Probstein 1966, p. 230).

The normalized or canonical velocity profile, f, which must assume the values ± 1 at $y = \pm\infty$ (see (2a)), is chosen to be

$$f = \tanh y. \tag{5b}$$

This profile is selected because it closely represents experimentally observed profiles and because its stability has been extensively studied by others as well (Blumen 1970; Blumen *et al.* 1975; Jackson & Grosch 1988). The actual base velocity profile, U, will depend on the Mach number, m_1, and on the temperature ratio, T_2, through the Howarth–Dorodnitsyn transformation; this important dependence was ignored by Blumen *et al.* (1975).

There are, of course, other choices for f (e.g. erf$y$, Lock profile (Gropengiesser 1969), etc.). The extension of our principal theoretical results to these other profiles requires minor modifications in the analysis (see §7). The introduction of the tanh profile makes the analysis more concrete and is, in any case, the one that will be used in our numerical computations because of its 'symmetry'.

Although key numerical results will be presented in §7, we need some information on them at this point to motivate the analysis. This information may be found in Jackson & Grosch (1988); above a certain Mach number, which depends on the temperature ratio T_2 and the obliqueness angle θ, a shear layer may sustain several instability modes. One of these modes has spatial growth rates of $O(1)$ and phase velocities (approximately) equal to zero. These modes have two surprising properties; the most unstable mode is two-dimensional and its maximum growth rate occurs at zero frequency. If these modes indeed exist, they are crucially important at large Mach numbers; but their very existence, and certainly their relevance have not been demonstrated convincingly (Jackson & Grosch promise to do so in a future study). Therefore, the analysis in this paper is *not* directed at these modes but, in fact, is directed at those other modes whose existence and relevance have been demonstrated by several authors (Gropengiesser 1969; Blumen *et al.* 1975; Jackson & Grosch 1988).

These latter pair of modes behave in a much more physical manner and are related to the well-known incompressible mode through 'mode splitting' (described in §7.1). At large Mach numbers, these modes have small growth rates and convection speeds which are (approximately) those of the two external streams. This implies that the critical layer moves progressively further into one of the external streams as the Mach number becomes large. It is convenient (but not essential, see for example Cowley & Hall 1990) to keep the critical layer at a finite point as $m_1 \to \infty$. Therefore, we introduce a one-to-one transformation via (5b) and consider f as our new *independent* variable. Then, after the introduction of a new *dependent* variable,

$$\mathscr{R} = \frac{(1-f^2)^{\frac{1}{2}}}{f-\hat{c}}p, \tag{6a}$$

the Rayleigh equation (1a) becomes

$$\frac{\mathrm{d}^2\mathscr{R}}{\mathrm{d}f^2} + \left[\frac{Q+1}{(1-f^2)^2} - \frac{2f}{(1-f^2)(f-\hat{c})} - \frac{2}{(f-\hat{c})^2}\right]\mathscr{R} = 0, \tag{6b}$$

where the quantity Q is still given by (1b). The compressible (unstable) modes of a mixing layer satisfy (6b) with the boundary condition $\mathscr{R} = 0$ at $f = \pm 1$; we always consider a neutral mode as the limit of an unstable mode when the growth rate of the latter tends to zero.

It is clear from the governing equation (6*b*), (1*b*) and (5*a*) and the boundary conditions that the functional dependence of the canonical eigenvalue is

$$\hat{c} = \hat{c}\{\kappa, \mu\cos^2\theta; [(\gamma-1)/2]\mu, T_2\}, \tag{7a}$$

where

$$\mu = (\tfrac{1}{2}m_1)^2. \tag{7b}$$

Thus, at a given wavenumber, there are three similarity parameters of which we shall only vary two, namely, m_1 and T_2 (and keep γ = const. = (1.4 for the numerical results)). There is a remarkably rich structure in this two-dimensional parameter space, which we shall study in the formal limit as $m_1 \to \infty$, T_2 = fixed = $O(1)$, $(\gamma-1)$ = fixed = $O(1)$, and κ = fixed = $O(1)$ but $\mu\cos^2\theta$ may be arbitrary (including zero). The case $\mu\cos^2\theta \gg 1$ is treated in the main part of the paper and the results for $\mu\cos^2\theta = O(1)$ are given in Appendix A.

Since $[\frac{1}{2}(\gamma-1)]$ is fairly small, the full asymptotic structure does not emerge until the Mach number becomes quite large (say, $m_1 > 10$). In an intermediate range, say, $m_1 \lesssim 4$, T is still of order unity but the coefficient of $\mathscr{R}$ in (6*b*) can still be dominated by the 'large' quantity $(\frac{1}{2}m_1\cos\theta)^2 = \mu\cos^2\theta$ in Q when $\theta \neq \frac{1}{2}\pi$. This suggests the limit $m_1 \to \infty$, $[\frac{1}{2}(\gamma-1)]\mu = O(1)$ associated with the name of Newton (Hayes & Probstein 1966, p. 129). However, it can be shown that the resulting modes would then have to be supersonic with respect to *both* external streams (see discussion in §7.3), and, therefore, could not represent the continuation (to high Mach numbers) of the most rapidly growing intermediate-Mach-number modes (Jackson & Grosch 1988). In addition, from the numerical results of Jackson & Grosch, it may be inferred that $\mu\cos^2\theta$ remains less than unity (i.e. this quantity is not large) for the most rapidly growing spatial modes in this intermediate-Mach-number range. Therefore, any sensible asymptotic limit in this range would have to be based on $m_1 \to \infty$ but $\mu\cos^2\theta = O(1)$. This, together with the Newtonian limit (i.e. $[\frac{1}{2}(\gamma-1)]\mu = O(1)$), provides no simplification at all. Thus, for our flow, it is meaningful to consider only the full hypersonic limit: $m_1 \to \infty$ with T_2 and $(\gamma-1)$ of order one. Our results will be valid for all obliqueness angles (including $\theta = \frac{1}{2}\pi$).

The flow develops a multilayer structure in our hypersonic limit, which is outlined in figure 1. We now consider each of these layers in turn.

3. The main shear layer

The results of Jackson & Grosch (1988) show that as $m_1 \to \infty$ there is a finite range of unstable wavenumbers. In this limit the base temperature profile (5*a*) is dominated by aerodynamic or viscous (or frictional) heating in the main part of the shear layer (where f is sufficiently different from ± 1) owing to the large mean velocity gradient there. This implies that the coefficient of $\mathscr{R}$ becomes quite large in (6*b*) [actually $O(m_1^4)$] and suggests that this equation can be solved by the WKBJ method.

To make this observation more precise, we must say something about the relative magnitude of $(f-\hat{c})$. Since the critical layer moves towards one of the external streams (i.e. one of the points $f = \pm 1$) as $m_1 \to \infty$, we define the main shear layer to be the region where $(f-\hat{c}) \neq o(1)$ (see figure 1).

We consider only the *slow mode* for which $\mathrm{Re}\,(c) \approx U_2$ (or equivalently $\mathrm{Re}\,(\hat{c}) \approx -1$) and show how this analysis is modified (trivially) for the fast mode which is characterized by $\mathrm{Re}\,(c) \approx U_1$ or $\mathrm{Re}\,(\hat{c}) = +1$. Here we use $\mathrm{Re}\,(\cdot)$ to denote the real part of a complex number and write $\hat{c} = \hat{c}_\mathrm{R} + \mathrm{i}\hat{c}_\mathrm{I}$. Typically, the imaginary part of the

eigenvalue is quite small at high Mach numbers; the base flow is only slightly unstable.

The WKBJ solution is of the form

$$\mathscr{R} = \exp(\kappa\mu\phi) \quad \text{for} \quad f < f_0, \tag{8a}$$

where the complex phase, ϕ, expands as

$$\phi = \phi^{(0)} + \phi^{(1)}/\mu + \phi^{(2)}/\mu^2 + \ldots. \tag{8b}$$

Here
$$\mu = (\tfrac{1}{2}m_1)^2 \gg 1 \tag{8c}$$

and we introduce the notation

$$T = \tfrac{1}{2}(\gamma-1)\mu(1-f^2) + T^{(0)}(f), \tag{8d}$$

with
$$T^{(0)}(f) = 1 - \tfrac{1}{2}(1-T_2)(1-f). \tag{8e}$$

Clearly $T^{(0)}$ is of order unity and represents the effect of the external (i.e. non-aerodynamic) heating of the mixing layer.

After substituting the Rytov transformation, (8a), into the governing equation (6b), and using expansions (8b, d), we arrive at $O(\mu^2)$:

$$\phi^{(0)} = \pm \int_f^{f_0} g(f)\,\mathrm{d}f + \phi_\pm^{(0)}, \tag{9a}$$

where
$$g(f) = [\tfrac{1}{2}(\gamma-1)]^{\frac{1}{2}} \frac{[\frac{1}{2}(\gamma-1)(1-f^2) - \cos^2\theta(f-\hat{c})^2]^{\frac{1}{2}}}{(1-f^2)^{\frac{1}{2}}}, \tag{9b}$$

and f_0 will be defined in a moment, and at $O(\mu)$:

$$\kappa\phi^{(1)} = -\tfrac{1}{2}\log g \mp \tfrac{1}{2}\kappa \int_f^{f_0} \frac{J(f)}{g(f)}\,\mathrm{d}f + \kappa\phi_\pm^{(1)}, \tag{10a}$$

where
$$J(f) = T^{(0)}(f)\frac{\cos^2\theta(f-\hat{c})^2 - (\gamma-1)(1-f^2)}{(1-f^2)^2} \tag{10b}$$

and $\phi_\pm^{(0)}$, $\phi_\pm^{(1)}$ are arbitrary constants of integration at this stage. These will be determined by the analysis which follows.

A few observations are now in order. First, the present result applies even when $\cos^2\theta = O(\mu^{-1})$ (i.e. for $\theta \approx \frac{1}{2}\pi$) and can easily be re-expanded in powers of μ^{-1} to obtain the 'properly' ordered result for this case. Second, the total wavenumber, κ, is assumed to lie in the range $\mu^{-1} \ll \kappa \ll \mu$, and finally $\hat{c}$ has *not* been expanded in powers of m_1 because $(f-\hat{c})$ is bounded away from zero and is $O(1)$ in the main shear layer (and the above results can always be re-expanded if necessary to take into account the dependence of $\hat{c}$ on the Mach number).

It turns out, however, that $\hat{c} = -1 + O(\mu^{-1})$ (see §6) so that as $\mu \to \infty$, the derivative of the lowest-order phase, $\mathrm{d}\phi^{(0)}/\mathrm{d}f = \mp g$, will have a simple zero at

$$f(y_0) = f_0 = -\frac{1-\nu}{1+\nu}, \tag{11a}$$

where
$$\nu = \frac{\gamma-1}{2\cos^2\theta}. \tag{11b}$$

For $\gamma = 1.4$ and $\theta = 0$, $f_0 = -\frac{2}{3}$. As the obliqueness angle increases, f_0 moves to the

right along the f-axis and finally moves out of the main shear layer region and into the external stream ($f \approx 1$) when $\cos^2\theta = o(1)$.

Therefore, $f_0 = f(y_0)$ is a first-order turning point of the WKBJ solution (see figure 1) when $\cos^2\theta = O(1)$; there is no WKBJ turning point when $\cos^2\theta = o(1) = O(\mu^{-1})$, say, because f_0 moves into the high-speed edge layer and the flow there must be rescaled (Appendix A).

In order to bring out the fact that the phase, $\phi^{(0)}$, is almost pure imaginary to the right of f_0 when $f_0 < 1$ (and for other purposes as well) it is convenient to write

$$\mathscr{R} = \exp(\mathrm{i}\kappa\mu\Phi) \quad \text{for} \quad f > f_0, \tag{12a}$$

with

$$\Phi = \Phi^{(0)} + \Phi^{(1)}/\mu + \Phi^{(2)}/\mu^2 + \ldots. \tag{12b}$$

The WKBJ formalism yields, in the spirit of the previous analysis of this section,

$$\Phi^{(0)} = \pm \int_1^f G(f)\,\mathrm{d}f, \tag{13a}$$

$$G(f) = \mathrm{i}g(f) = [\tfrac{1}{2}(\gamma-1)]^{\frac{1}{2}} \frac{[\cos^2\theta(f-\hat{c})^2 - \tfrac{1}{2}(\gamma-1)(1-f^2)]^{\frac{1}{2}}}{(1-f^2)^{\frac{1}{2}}} \tag{13b}$$

and

$$\mathrm{i}\kappa\Phi^{(1)} = -\tfrac{1}{2}\log G \pm \tfrac{1}{2}\mathrm{i}\kappa \int_0^f \frac{J(f)}{G(f)}\,\mathrm{d}f + \mathrm{i}\kappa\Phi_{\pm}^{(1)}, \tag{13c}$$

where $\Phi_{\pm}^{(1)}$ are constants of integration and $J(f)$ is defined by (10b). Note that the lower limit of integration in (13a) is chosen in such a way that it will be fairly easy to satisfy the boundary condition at $f = 1$ and that G has an integrable singularity at this point.

Thus there are two WKBJ solutions – one for each side of the turning point – when $f_0 \neq 1$ (i.e. when $0 \leqslant \theta < \frac{1}{2}\pi$), which are analytic continuations of each other and are related by a 'connection formula' across the transition region, $f \approx f_0$. The nature and physical interpretation of this transition region and the corresponding connection formula (which is almost classical) will be discussed in §5. This discussion can be made rather short if we first find out which linear combination of (13a) may exist for $f > f_0$; this is done by satisfying the boundary condition at $f = 1$.

4. The high-speed edge layer

There is a difficulty in the upper external stream with WKBJ solution, (13c), because the integrand has a $(-\frac{3}{2})$ singularity at $f = 1$. Physically, the problem arises from the fact that aerodynamic heating is unimportant in the external stream (a uniform flow) so that the basic premise which guarantees the existence of the WKBJ solution in the main layer is violated. Therefore, this solution cannot satisfy the boundary condition at $f = 1$.

The base temperature profile, (5a), clearly reveals the difficulty mathematically; although $\mu = (\frac{1}{2}m_1)^2$ is large, $(1-f^2)$ is small near $f = 1$. This observation suggests the introduction of a scaled edge-layer coordinate

$$\frac{\xi}{\mu} = 1 - f, \tag{14}$$

where the edge layer is defined by $\xi = O(1)$ (see figure 1). In this layer $(f-\hat{c}) = O(1)$. A similar rescaling was used in the hypersonic boundary-layer analysis of Cowley &

Hall (1990). One might suppose that there is another edge layer (of the type we shall be describing in this section) in the low-speed stream, near $f=-1$; this supposition is incorrect because the latter contains the critical layer and the flow behaves quite differently there.

In order to re-express the governing equation, (6*b*), in terms of the upper edge-layer coordinate, ξ, we note that the temperature distribution may be written

$$T = T_e^{(0)} + T^{(1)}/\mu, \tag{15a}$$

where

$$T_e^{(0)} = 1 + (\gamma - 1)\,\xi, \tag{15b}$$

$$T^{(1)} = -\tfrac{1}{2}(\gamma-1)\,\xi^2 - \tfrac{1}{2}(1-T_2)\,\xi \tag{15c}$$

and a direct substitution of (15) into the quantity Q, (1*b*), yields

$$Q = \kappa^2[\mu T_e^{(0)} \cos^2\theta(1-\hat{c})^2 - T_e^{(0)2} - Q^{(0)}\cos^2\theta + O(\mu^{-1})], \tag{16a}$$

where

$$Q^{(0)} = 2T_e^{(0)}(1-\hat{c})\,\xi - T^{(1)}(1-\hat{c})^2. \tag{16b}$$

Therefore, the governing equation, (6*b*), may be written in terms of the edge-layer variable and the above expansions as

$$\frac{\mathrm{d}^2\mathscr{R}}{\mathrm{d}\xi^2} + \frac{1}{4\xi^2}\{\mu\kappa^2 T_e^{(0)}\cos^2\theta(1-\hat{c})^2 + 1 - \kappa^2 T_e^{(0)2} + \mathscr{Q}^{(0)}\cos^2\theta + O(\mu^{-1})\}\,\mathscr{R} = 0, \tag{17a}$$

where

$$\mathscr{Q}^{(0)} = -\kappa^2[Q^{(0)} - \xi T_e^{(0)}(1-\hat{c})^2]. \tag{17b}$$

The presence of the large parameter $\mu = (\tfrac{1}{2}m_1)^2$ implies that (17*a*) may be solved by the WKBJ method. After writing

$$\mathscr{R} = \exp(\mathrm{i}\mu^{\frac{1}{2}}\Psi) \tag{18a}$$

and expanding

$$\Psi = \Psi^{(0)} + \Psi^{(\frac{1}{2})}/\mu^{\frac{1}{2}} + O(\mu^{-1}) \tag{18b}$$

we find in a straightforward manner that the lowest-order phase is

$$\Psi^{(0)} = \pm F(\xi), \tag{18c}$$

where

$$F(\xi) = \tfrac{1}{2}k(1-\hat{c})\left\{2T_e^{(0)\frac{1}{2}} + \log\frac{T_e^{(0)\frac{1}{2}}-1}{T_e^{(0)\frac{1}{2}}+1}\right\}. \tag{18d}$$

The next order correction to the phase, given by the classical result

$$\mathrm{i}\Psi^{(\frac{1}{2})} = -\tfrac{1}{2}\log\frac{\mathrm{d}F}{\mathrm{d}\xi} = -\tfrac{1}{2}\log\left\{\tfrac{1}{2}k(1-\hat{c})\frac{T_e^{(0)\frac{1}{2}}}{\xi}\right\}, \tag{18e}$$

arises because our dependent variable is $\mathscr{R}$ (rather than p); for the pressure the correction to the phase at this order is zero as may be seen from (1) by considering the solution at $y=+\infty$. The term in the curly brackets of (18*d*) behaves as $[\log\xi + \text{const.} + O(\xi)]$ as $\xi\to 0$, or as $(-2y + \text{const.} + \text{exponentially small terms})$ as $y\to+\infty$. Therefore, in order to satisfy boundedness in the upper uniform stream, we must take the upper sign in (18*c*) for unstable temporal modes ($\hat{c}_1 > 0, k > 0$); for unstable spatial modes this choice must also hold by analytic continuation. Putting these results together, we find that at large Mach numbers the solution in this edge layer may be written

$$\mathscr{R} = \exp[\mathrm{i}\mu^{\frac{1}{2}}F - \tfrac{1}{2}\log(\mathrm{d}F/\mathrm{d}\xi) + O(\mu^{-\frac{1}{2}})]. \tag{19}$$

We emphasize that (19) satisfies the correct boundary condition at $\xi = 0$ (or $f = 1$ or

$y = +\infty$) and that the arbitrary constant of integration in the phase has been ignored because the (complex) amplitude of an instability mode is arbitrary, and this integration constant may be absorbed into the amplitude.

There remains to show that our edge-layer solution, (19), matches (in an asymptotic sense) with the solution in the main layer in the region $f > f_0$. Since the procedure is mostly algebraic, we omit the details. There are, however, a couple of points worth noting. First, because the edge-layer solution consists of a single exponential, it appears likely that only one of the WKBJ solutions in (13) is needed. We write the required solution (with hindsight) as

$$\mathscr{R} = \exp\left[-\mathrm{i}\kappa\mu\int_1^f G(f)\,\mathrm{d}f - \tfrac{1}{2}\log G(f) - \tfrac{1}{2}\mathrm{i}\kappa\int_0^f \frac{J(f)}{G(f)}\,\mathrm{d}f + \mathrm{i}\kappa\Phi_-^{(1)} + O(\mu^{-1})\right] \tag{20}$$

where, in order to succeed with the asymptotic matching, we must allow $\Phi_-^{(1)} = O(1)$ to depend on $\log\mu$.

In order to carry out the matching (Van Dyke 1975, p. 93), we recall that both integrands in (20) are singular as $f \to 1$, and we must first peel off this singularity in order to find the outer limit of (20); this is what produces the fractional powers of μ in (19). The final result is

$$\mathrm{i}\kappa\Phi_-^{(1)} = \tfrac{1}{4}\log\mu - \tfrac{1}{2}\log\kappa - \mathrm{i}\kappa\hat{J}(0) + \tfrac{1}{2}\mathrm{i}\kappa\int_0^1 \frac{\hat{J}(\xi)-\hat{J}(0)}{\xi^{\frac{3}{2}}}\,\mathrm{d}\xi, \tag{21a}$$

with

$$\hat{J}(\xi) = \frac{J(1-\xi)}{G(1-\xi)}\xi^{\frac{3}{2}} \tag{21b}$$

and $\hat{J}(0) = \hat{J}(\xi \to 0)$. This asymptotic matching shows how the boundary condition at $f = 1$ is transmitted to the main layer through the intervening edge layer.

We now have a solution that satisfies the correct boundary condition (for any $\hat{c}$ at this point) in the upper external stream and is valid almost all the way to the turning point, $f = f_0$ (see figure 1). In the following section we shall develop the connection formula across the turning point which will provide the relationship between the two sets of WKBJ solutions in the main layer; (8*a*) and (12*a*). Note, however, that implicit in our derivation in this section is the assumption $\mu\cos^2\theta \gg 1$ (see (17*a*)). When the instability wave is very oblique (i.e. $\mu\cos^2\theta = O(1)$), the transonic region and the high-speed edge layer fall on top of each other and a different solution to (17*a*) must be sought; this is done in Appendix A. Physically speaking, in this case the flow over most of the shear layer behaves subsonically (because of the 'sweepback' effect due to obliqueness) and it is only in the upper external stream where the flow may become supersonic (relative to the instability wave). Actually, even if the flow remains subsonic in the upper stream (e.g., $\theta = \frac{1}{2}\pi$), an extra layer is required because the main WKBJ solution, (10*a*), becomes singular at $f = 1$.

5. The transonic layer

Consider the case $f_0 < 1$ (i.e. $\theta \neq \frac{1}{2}\pi$) so that the transonic layer or the WKBJ turning point lies in the central part of the mixing layer. In order to explain the structure of the relevant eigenfunction, we first summarize our results for the slow mode (whose phase speed is approximately U_2; figure 2) in physical terms. The relative Mach number, $(U_1 - c_R)/a_1 \approx (U_1 - U_2)/a_1 = m_1$, is large so that for $y > y_0 =$

$\tanh^{-1} f_0$ the flow relative to the instability wave is highly supersonic. Since the growth rate is very small, this supersonic flow is essentially steady in the reference frame of the instability mode; thus it is characterized by Mach waves which lie nearly parallel to the x-axis. The vertical distance, d, between 'successive' Mach waves is $O(\lambda/m_1)$ which is assumed to be small with respect to the cross-stream lengthscale of the base velocity profile (which is $O(1)$). The characteristic wavelength of the disturbance is denoted by λ. Therefore, as we traverse the flow in the $(+y)$-direction in this upper region, we encounter a series of Mach lines separated by a small distance d; in mathematical terms this is represented by the rapidly oscillating WKBJ solution (12). For an unstable mode, the strength of the Mach waves actually decays slowly.

On the other hand, in the lower region $y < y_0$, the relative Mach number, $(c_R - U_2)/a_2 \approx (U_2 - U_2)/a_2 = 0$, is quite small so that the flow there is nearly incompressible and is characterized by exponentially growing and decaying solutions (as opposed to oscillatory solutions; see (8)). Clearly, in an intermediate region around $y = y_0$ (or $f = f_0$), the flow must change from an oscillatory one to an exponential one (see figure 1); this occurs in the turning point region of the WKBJ solution or, physically, in the transonic region that bridges these high- and low-Mach-number flows. We next analyse the characteristics of this transonic layer.

Introduce an inner variable

$$\eta = \frac{f_0 - f}{\delta}, \tag{22a}$$

where $\eta = O(1)$ in the transonic layer and δ is its characteristic thickness. Observe that the largest term in the coefficient of $\mathscr{R}$ in (6b) is $O(T^2) = O(\mu^2)$ in the main layer, and this implies the scaling, in analogy with the classical turning point problem (Nayfeh 1973, p. 336),

$$\delta = \mu^{-\frac{2}{3}} = (\tfrac{1}{2}m_1)^{-\frac{4}{3}} \ll 1. \tag{22b}$$

After writing (6b) in terms of this inner variable and expanding its coefficient in Taylor series about $\eta = 0$, we arrive at

$$\frac{\mathrm{d}^2\mathscr{R}}{\mathrm{d}\eta^2} + [-A\eta + \mu^{-\frac{1}{3}}B + O(\mu^{-\frac{2}{3}})]\,\mathscr{R} = 0, \tag{23a}$$

where

$$A = \text{const.} = \tfrac{1}{2}\kappa^2 \frac{(\gamma-1)^2}{1-f_0^2}, \tag{23b}$$

$$B = \text{const.} = \kappa^2 J(f_0), \tag{23c}$$

with J defined by (10b) and f_0 denoting the turning point, (11). The present turning-point problem is distinguished from the classical one by the presence of the $O(\mu^{-\frac{1}{3}})$ term in (23a); this arises from the fact that, in the main layer, the coefficient of $\mathscr{R}$ in (6b) also contains a term of $O(\mu)$. Since the growth rates are small, κ^2 is almost (pure) real and positive and the rest of the analysis in this section is carried out with this limitation in mind (so that we do not have to treat (23a) as an equation in the complex η-plane and worry about Stokes lines). It should be noted, however, that our results are valid throughout the region $\mathrm{Re}\,(\kappa) > 0$; in a narrow boundary layer of thickness $O(\mu^{-1})$ in vicinity of the imaginary axis our results fail for one of two reasons. If $\mathrm{Im}\,(\kappa) = O(\mu^{-1})$ (i.e. the total wavenumber is approximately zero), $\kappa^2 T^2$ is no longer large and we essentially have the theory of Cowley & Hall (1990), while for $\mathrm{Im}\,(\kappa) = O(1)$, the asymptotic expansion of (23a) for large η differs from the one we shall employ because of the presence of Stokes lines when $\kappa = \mathrm{i}\kappa_1$ = pure imaginary.

To solve the governing equation, (23*a*), in the transonic layer, we write the two-term solution

$$\mathscr{R} = \mathscr{R}^{(0)} + \mu^{-\frac{1}{3}}\mathscr{R}^{(\frac{1}{3})} + O(\mu^{-\frac{2}{3}}) \tag{24a}$$

and find

$$\mathscr{R}^{(0)} = \alpha^{(0)}\,\mathrm{Ai}\,(\eta A^{\frac{1}{3}}) + \beta^{(0)}\,\mathrm{Bi}\,(\eta A^{\frac{1}{3}}), \tag{24b}$$

where Ai and Bi are Airy functions in the notation of Abramowitz & Stegun (1970, p. 446). Based on our previous remarks, A = const. is (almost) real and positive and the $\frac{1}{3}$-power in (24*b*) is given by the usual cube root; $[\alpha^{(0)}, \beta^{(0)}]$ are constants. $\mathscr{R}^{(\frac{1}{3})}$ obeys an inhomogeneous Airy equation (the forcing terms are Airy functions) whose particular solution may be found by the method of variation of parameters. This solution is needed to carry out the asymptotic matching with the WKBJ solutions in the main shear layer to the order of accuracy to which the latter are written! A particular solution, $\mathscr{R}^{(\frac{1}{3})}_{*}$, and its asymptotic behaviour for large $|\eta|$ is given in Appendix B. We next write the two term solution in the transonic layer as

$$\mathscr{R} = \alpha^{(0)}[1+\mu^{-\frac{1}{3}}\alpha^{(\frac{1}{3})}]\,\mathrm{Ai}\,(\eta A^{\frac{1}{3}}) + \beta^{(0)}[1+\mu^{-\frac{1}{3}}\beta^{(\frac{1}{3})}]\,\mathrm{Bi}\,(\eta A^{\frac{1}{3}}) + \mu^{-\frac{1}{3}}\mathscr{R}^{(\frac{1}{3})}_{*} \tag{25}$$

with the understanding that $\alpha^{(0)}$ and $\beta^{(0)}$ are of the same order; $\alpha^{(\frac{1}{3})} = O(1)$ and $\beta^{(\frac{1}{3})} = O(1)$ are constants. With the help of Appendix B, we match this two-term transonic solution to the two WKBJ solutions in the main shear layer to determine some of the constants of integration in (9) and (10). The final results are

$$\phi^{(0)}_{+} = -\mathrm{i}\int_{1}^{f_0} G(f)\,\mathrm{d}f, \tag{26a}$$

$$\kappa\phi^{(1)}_{+} = -\tfrac{1}{2}\mathrm{i}\kappa\int_{0}^{f_0}\frac{J(f)}{G(f)}\mathrm{d}f + \mathrm{i}\kappa\Phi^{(1)}_{-} + \tfrac{1}{4}\mathrm{i}\pi, \tag{26b}$$

where $\Phi^{(1)}_{-}$ is defined by (21*a*). Note that there is no special significance of the zero in the lower limit of the integral in (26*b*) and, in fact, it may be replaced by any other (convenient) point provided that this is done in all the lower limits which are now set to zero.

Tacit in our derivation is the fact that any oscillatory solution in the supersonic region can only be matched onto an exponentially growing solution (as $f \to -1$) in the subsonic regime; the 'amplitude' of the exponentially decaying solution is *not* determined by our (or the classical) connection formulae. In other words, these formulae are directional in character in the sense that the validity of the right-hand sides of (26) imply the validity of the left-hand sides (but not conversely); therefore, the equal signs in (26) should really be replaced by arrows pointing to the left to remind us of the one-way nature of these formulae (Kemble 1935). For this reason the integration constants $\phi^{(i)}_{-}$ $(i = 0, 1)$ in (9*a*) and (10*a*) cannot be determined by the matching across the transonic layer.

For completeness we also give the flow field in the transonic layer by quoting expressions for the relevant coefficients

$$\alpha^{(0)} = -\mathrm{i}\frac{(\pi\kappa)^{\frac{1}{3}}}{A^{\frac{1}{6}}\delta^{\frac{1}{4}}}\mathrm{e}^{\mathrm{i}\pi/4}D, \tag{27a}$$

$$\beta^{(0)} = \frac{(\pi\kappa)^{\frac{1}{3}}}{A^{\frac{1}{6}}\delta^{\frac{1}{4}}}\mathrm{e}^{\mathrm{i}\pi/4}D, \tag{27b}$$

where

$$D = \exp\left[-\mathrm{i}\kappa\mu\int_{1}^{f_0} G(f)\,\mathrm{d}f - \tfrac{1}{2}\mathrm{i}\kappa\int_{0}^{f_0}\frac{J(f)}{G(f)}\mathrm{d}f + \mathrm{i}\kappa\Phi^{(1)}_{-}\right] \tag{27c}$$

and $[\alpha^{(\frac{1}{3})}, \beta^{(\frac{1}{3})}]$ are (unfortunately) undetermined at this order of matching.

6. The low-speed edge layer (critical layer)

We have now shown that the dependent variable, $\mathscr{R}$, ultimately exhibits exponential growth as $f \to -1$ in the main shear layer for all $f_0 \leqslant 1$ ($f = f_0$ defines the location of the transonic region).

It is clear that the subsonic WKBJ solution cannot satisfy the boundary condition $\mathscr{R} = 0$ at $f = -1$ and another boundary layer has to be inserted in the vicinity of $f \approx -1$ (see figure 1). This layer contains the critical layer whose importance in stability theory is well known (Betchov & Criminale 1967; Drazin & Reid 1981).

As in the case of the high-speed edge layer (§4), the base temperature profile, (5a), suggests the scaling

$$\frac{\zeta}{\mu} = 1 + f, \tag{28}$$

where $\zeta = O(1)$ defines this layer whose width is $O(\mu^{-1})$. Since the canonical eigenvalue $\hat{c} \approx -1$, $(f - \hat{c}) = [\zeta/\mu - (1 + \hat{c})]$ will be small in this layer, and we must say something about the relative magnitude of this quantity.

We do this by specifying the behaviour of $\hat{c}$ as a function of μ. The natural expansion

$$\hat{c} = -1 + \sigma/\mu + O(\mu^{-2}); \quad \sigma = O(1) \tag{29}$$

of the eigenvalue, in terms of the Mach number, leads to a self-consistent theory. The dependent variable $\mathscr{R}$ expands like

$$\mathscr{R} = \mathscr{R}_c^{(0)} + O(\mu^{-1}). \tag{30}$$

Substituting (28) to (30) into Rayleigh's equation, (6b), and collecting coefficients of like powers of μ, we obtain the lowest-order edge-layer equation

$$\frac{\mathrm{d}^2 \mathscr{R}_c^{(0)}}{\mathrm{d}\zeta^2} + \left\{ \frac{1 - \kappa^2 T_c^{(0)^2}}{4\zeta^2} + \frac{1}{\zeta(\zeta - \sigma)} - \frac{2}{(\zeta - \sigma)^2} \right\} \mathscr{R}_c^{(0)} = 0, \tag{31a}$$

where

$$T_c^{(0)} = T_2' + (\gamma - 1)\zeta. \tag{31b}$$

In order to satisfy boundary conditions at $\zeta = 0$ and to perform the matching with the WKBJ solution, we must examine the solutions of (31a) for small and large ζ. When $\zeta \to 0$,

$$\frac{\mathrm{d}^2 \mathscr{R}_c^{(0)}}{\mathrm{d}\zeta^2} + \left\{ \frac{1 - \kappa^2 T_2^2}{4\zeta^2} + O(\zeta^{-1}) \right\} \mathscr{R}_c^{(0)} = 0, \tag{32}$$

which has the solutions $\zeta^{n_\pm}$, where

$$n_\pm = \tfrac{1}{2}(1 \pm \kappa T_2'). \tag{33}$$

It therefore follows from (5b), (6a), (28), (29) and (33) that

$$p \sim \zeta^{-\frac{1}{2}} \mathscr{R} \sim \zeta^{\pm \kappa T_2'/2} \sim \mathrm{e}^{\pm \kappa T_2' y} \quad \text{as} \quad \zeta \to 0 \quad (\text{or } y \to -\infty). \tag{34}$$

This shows that $\mathscr{R}_c^{(0)}$ can be made to satisfy the proper (i.e. decaying or 'subsonic') boundary condition at $\zeta = 0$ (or $y = -\infty$) by choosing the plus sign in (33) so that we must set

$$\mathscr{R}_c^{(0)} = 0 \quad \text{at} \quad \zeta = 0. \tag{35}$$

The lower sign in (33) is inadmissible.

In our numerical calculations we enforce a strong version of (35) by requiring the

difference between the analytically and numerically calculated values of $\mathscr{R}_c^{(0)}$ to be of order ζ^4 in the vicinity of $\zeta = 0$. In other words, in the numerical procedure, we actually specify how $\mathscr{R}_c^{(0)}$ tends to zero in the lower external stream; this is done to exclude the term ζ^n- which may also vanish as $\zeta \to 0$ for small κT_2.

We call $\mathscr{R}_c^{(0)}$ the one-term inner (i.e. low-speed edge-layer) solution. The two-term outer expansion of this in terms of the main layer variable, $f = \zeta/\mu - 1$, is readily deduced from (31*a*) by re-expressing this equation in terms of f, and then solving the latter equation to two-term accuracy as $\mu \to \infty$. The final result, re-expressed in terms of the edge-layer variable, ζ, is

$$\mathscr{R}_c^{(0)} \to \exp\left[-\kappa\tfrac{1}{2}(\gamma-1)(\zeta-\mu) - \tfrac{1}{2}\kappa T_2(\log\zeta - \log\mu) + \epsilon_-\right], \tag{36}$$

where $\epsilon_- = \epsilon_-(\mu) = \text{const}$. Now (36) must match with the one-term inner expansion of the two-term WKBJ solution, (8), (9) and (10). This is indeed the case; the algebraic details, which are needed to determine $\epsilon_-(\mu)$, are relegated to Appendix C. Note that in (36) we retain only the exponentially decaying solution coming out of the low-speed edge layer (as $\zeta \to \infty$) because it is only this solution that matches with the exponentially growing WKBJ solution (as $f \to -1$) present in the main layer.

A most interesting result of our analysis is that the scaled eigenvalue σ (recall $\hat{c} = -1 + \sigma/\mu + \ldots$) is determined *entirely* by the low-speed edge layer; specifically (31*a*), boundary conditions (35) as $\zeta \to 0$ and (36) as $\zeta \to \infty$. The last boundary condition states that the lowest-order solution in the low-speed edge layer decays exponentially as we move into the main shear layer. The eigenvalue problem has now been completely decoupled from the behaviour of the eigenfunction in the rest of the shear layer because of the homogeneous boundary conditions associated with $\mathscr{R}_c^{(0)}$. A similar decoupling was found by Cowley & Hall (1990). The instability is, therefore, entirely dominated by the base flow in the vicinity of the lower external stream (for the slow mode).

7. Discussion and conclusions

An interesting result of our asymptotic theory is a simple high-Mach-number (i.e. hypersonic) similarity rule for instability waves in a mixing layer. This will be derived in §7.3; we begin our discussion with more general remarks and numerical results on the instabilities of compressible mixing layers. The latter are given for our base velocity profile with $U_1 = 1$ and $U_2 = 0$.

A secondary purpose of this paper is to discuss certain results relating to mode splitting and obliqueness. These results are *not* based on our asymptotic theory; they are obtained by numerically solving the full Rayleigh equation (at any Mach number). This numerically oriented study provides the explanation for the presence of the slow and fast modes (which are essential to our high-Mach-number asymptotic theory) and elucidates the role of oblique modes over a very large range of Mach number (much larger than what exists in the literature).

7.1. *Mode splitting and Miles' theory*

For two-dimensional modes ($\theta = 0$) in an isothermal mixing layer ($T_2 = 1$), the critical Mach number, m_1^*, introduced by Jackson & Grosch (1988) is $m_1^* \approx 1.84$. There is one unstable mode, whose phase speed is $U_m = \frac{1}{2}(U_1 + U_2)$, when $m_1 < m_1^*$. On the other hand, for $m_1 > m_1^*$ there are two unstable modes. We remark that the range of (unstable) wavenumbers and the maximum growth rates become increasingly

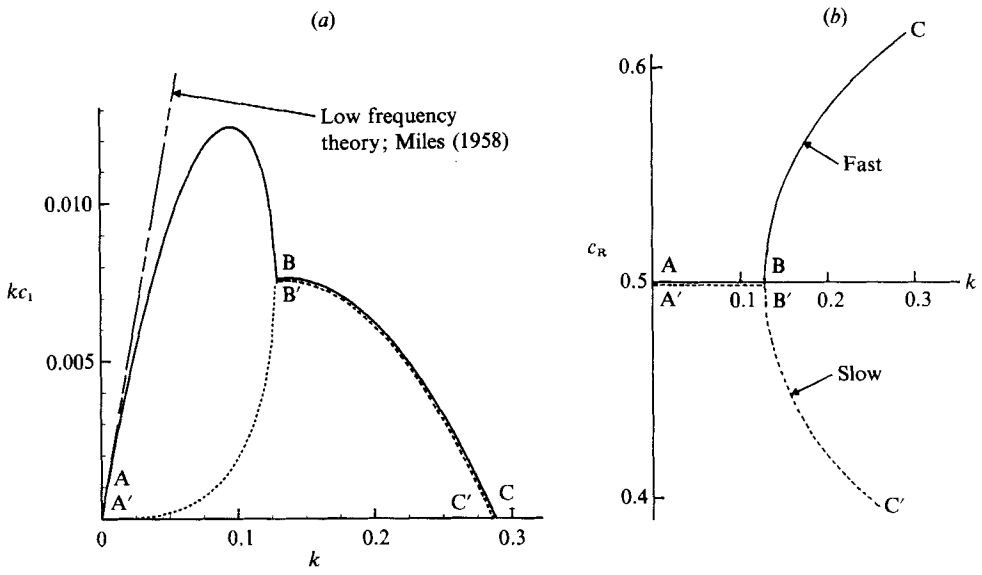

FIGURE 3. (*a*) Growth rate and (*b*) phase speed as a function of wavenumber. $m_1 = 2$, $T_2 = 1$, $\theta = 0$; ——, fast mode; – – – –, slow mode.

smaller as the mixing layer becomes more compressible in the Mach-number range $m_1 < m_1^*$. For reference, in the incompressible limit, the maximum temporal growth rate is 0.0949 and the range of unstable wavenumbers is the interval $(0, 1)$.

A typical result for the growth rates associated with the slow and fast modes is shown in figure 3(*a*). Because the base velocity profile $U - U_m = \frac{1}{2}\Delta U \tanh y$ is antisymmetric in y, both the slow and the fast modes have the same neutral wavenumber. For $m_1 \geqslant 2$, the segment $A'B'$ of the slow mode starts at the origin, while for $m_1^* < m_1 < 2$, the point A' is at a finite positive wavenumber. Thus, for $m_1 \geqslant 2$ we have two modes at vanishingly small wavenumbers (i.e. in the vortex-sheet limit); one of these is unstable (or possibly neutrally stable at sufficiently large Mach numbers – see discussion below) and the other is always neutrally stable. On the other hand, for $m_1 < 2$ we have one unstable mode at very small wavenumbers because A' is at a finite wavenumber. This agrees with the findings of Miles (1958), whose vortex-sheet result for the unstable mode is also indicated in the figure. We note that for Mach numbers less than the critical one, the slow mode disappears and the five points B, C, A', B', and C' are coincident at the neutral wavenumber. At m_1^* these points split apart to form a configuration whose general features are shown in figure 3(*a*).

For both the slow and fast modes the phase speed (figure 3*b*) is $c_R = U_m = 0.5$ when the wavelength is fairly long; evidently instability waves of this type feel the entire mixing layer and adjust their phase speeds accordingly (which, in this example, is U_m by antisymmetry). On the other hand, when the wavelengths become shorter, only part of the mixing layer is felt by the wave; therefore, instability waves with different phase speeds may be sustained by different parts of the mixing layer. Note that the phase speed of the neutral mode does not coincide with the fluid velocity at the (generalized) inflection point (which, by symmetry, is at $y = 0$). Therefore, we have irregular neutral modes; these are obtained as limits of unstable modes as their growth rates tend to zero.

As the Mach number is increased, the segment AB, along which the phase speed is

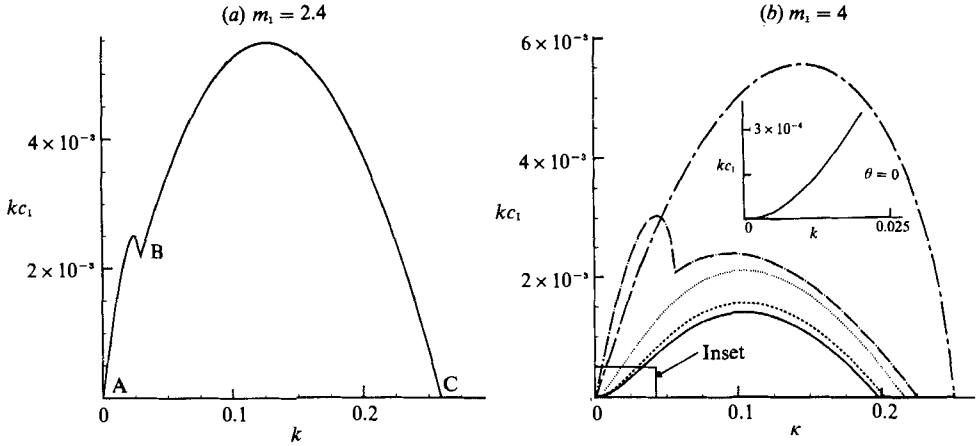

FIGURE 4. Growth rates at two Mach numbers. $T_2 = 1$: ——, $\theta = 0$; – – –, 20°; ....., 40°; —·—·—, 60°; ———, 80°.

equal to the average shear-layer speed, decreases in length, and at $m_1 = 2\sqrt{2}$ the point B reaches the origin (figure 4*a* shows the geometry for the growth rate just before this happens). For even larger Mach numbers, the section AB is absent altogether (i.e. the growth rate curve no longer has two local maxima) and the slope at the origin is zero. This is again consistent with Miles' vortex sheet theory which predicts stability above a Mach number of $2\sqrt{2}$.

We are now in a position to generalize the above remarks to heated mixing layers and to oblique modes. The main effect of external heating is the elimination of the perfect antisymmetry in the base flow. For example, the slow and the fast modes now have different neutral wavenumbers and the sharp corners (at $B = B'$ of figure 3) become gradually changing curves. Essentially, curves BC and $B'C'$ separate. Since the Mach number (i.e. m_1^*) at which the second mode emerges is quite close to the Mach number at which the growth rate curve of this mode intersects the origin (i.e. 1.84 versus 2 for isothermal flows) we propose the latter as a rule of thumb for the former. Thus, after Miles (1958), $m_1^* \approx 1 + T_2^{\frac{1}{2}}$; a simple result which agrees quite well with the (limited) numerical calculations of Jackson & Grosch (1988). Our formula for m_1^* implies that at this point $(U_1 - c_R)/a_1 = (c_R - U_2)/a_2 = 1$.

It is important to realize that all of our previous discussions are also relevant to spatial modes. As with external heating, spatial modes eliminate the perfect symmetry of the base flow; the various singularities (i.e. sharp corners) associated with temporal modes become smooth because, for spatial modes, these singularities are 'continued' into the complex wavenumber plane. A comparison between spatial and temporal calculations is shown in figure 5; the fast mode in both calculations exhibits a 'camelback' shape which has its origin in the mode splitting shown in figure 3(*a*).

A more quantitative comparison between these spatial and temporal calculations (figure 5) yields the following results. For the fast mode, the maximum temporal growth rate is 7.93×10^{-3} at $k \approx 0.149$. Via the Gaster (1962) transformation, the corresponding spatial growth rate is 1.04×10^{-2} at a frequency of 0.102. The respective numbers for the slow mode are 2.75×10^{-3} at $k \approx 0.078$ and 6.5×10^{-3} at $-\omega_I \approx 4.2 \times 10^{-2}$. It is seen that the Gaster transformation gives remarkably accurate results; the only difficulty is that in the spatial case, the maximum growth

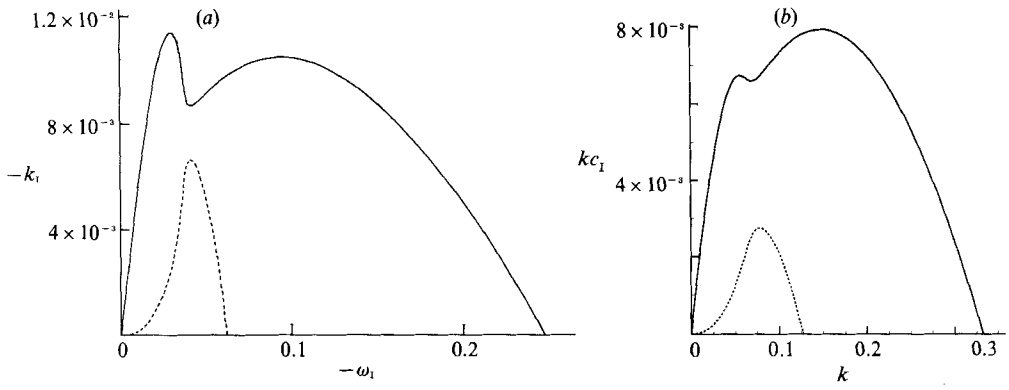

FIGURE 5. Comparison of (*a*) spatial (Jackson & Grosch 1988) and (*b*) temporal growth rates. $m_1 = 2.5$, $T_2 = 2$, $\theta = 0$: ——, fast mode; – – –, slow mode.

rate of the fast mode is still dominated by the first hump (but only slightly so). This is because for this combination of Mach number and temperature ratio we are still quite close to mode splitting, which, according to our approximate formula, occurs at $m_1^* = 1 + T_2^{\frac{1}{2}} \approx 2.41$.

Note that when the symmetry of the base flow is broken (i.e. heating or spatial modes) the first hump (see AB of figure 3*a*) need not disappear when the growth rate curve of the slow mode reaches the origin. This is because B and B' are generally separate points.

7.2. *The effect of obliqueness*

It is known that oblique modes frequently have the largest growth rates in compressible mixing layers (Gropengiesser 1969; Jackson & Grosch 1988). This is physically plausible because there are two distinct effects associated with obliqueness: (i) a general reduction of maximum growth rates (as in incompressible flows) because the effective base velocity difference, which induces the instability, becomes smaller by a factor of $\cos\theta$, and (ii) the effective Mach number also changes by this factor owing to the 'swept leading edge' of the instability wave. Since incompressible waves are usually more unstable than compressible ones, the second effect may completely offset the first one; the net result is the presence of a distinct oblique mode with the largest growth rate (figure 4*b*).

At moderate Mach numbers (say, $m_1 \lesssim 4$, when the variations in aerodynamic heating are unimportant owing to the small $\frac{1}{2}(\gamma - 1)$ factor in (5*a*)) the principal effect of obliqueness is to change the effective Mach number to $m_1 \cos\theta$ (from m_1) because of the 'sweep' of the phase fronts of a mode. In figure 4(*b*), for $\theta = 0$, we see something very similar to that discussed in the previous subsection (the inset shows the behaviour and the zero slope very near $k = \kappa = 0$); while for $\theta = 60°$ ($m_1 \cos\theta = 2$) the results remind us of those in figure 3(*a*) and, at $\theta = 80°$, ($m_1 \cos\theta = 0.69$) we see the familiar inverted U-shape that characterizes the instability of low-Mach-number flows.

The situation is, however, far more intricate, especially at higher Mach numbers where aerodynamic heating plays an important role. For example, for $m_1 = 8$ and $T_2 = 1$, a wide range of oblique waves ($0 \leqslant \theta \leqslant 60°$) has roughly (within 3%) the same peak growth rate (figure 6*a*). Furthermore, one of the principal results of our

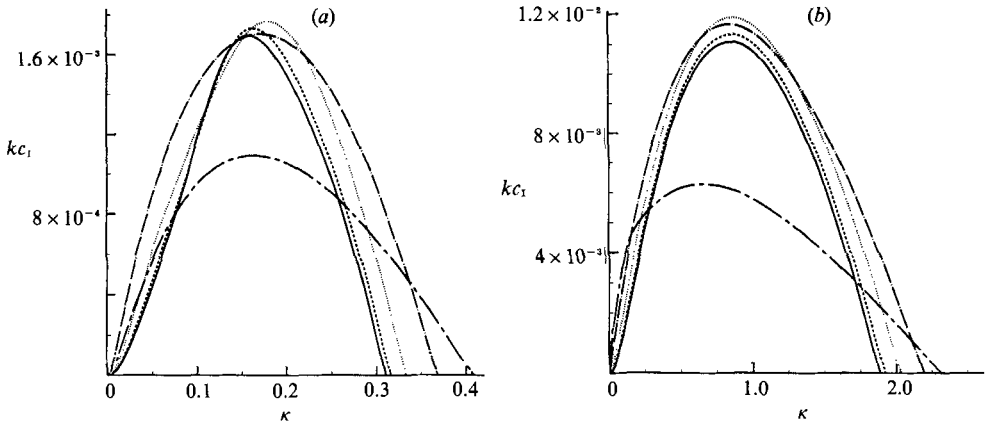

FIGURE 6. Growth rates of oblique modes: (*a*) $m_1 = 8$, $T_2 = 1$; (*b*) $m_1 = 4$, $T_2 = 0.2$: ——, $\theta = 0$; – – –, 20°; ....., 40°; —·—·—, 60°: ————, 80°.

asymptotic theory is that at even higher Mach numbers two-dimensional modes (with $\theta = 0$) are the most unstable (see §7.3).

This entire discussion on the behaviour of oblique modes is dependent on the temperature ratio, T_2. As seen from figure 6(*b*), in the presence of a substantial heating of the fast stream (at $y = +\infty$) (or a cooling of the slow stream at $y = -\infty$), even at moderate Mach numbers we have a wide range of oblique modes with roughly the same maximum growth rate (within 8%). Therefore, one must interpret with considerable caution one of the principal conclusions of previous investigators, such as Jackson & Grosch (1988) who state: 'we also find, in agreement with previous studies, that the maximum growth rate for any T_2 and m_1 occurs for three-dimensional modes'.

7.3. *High-Mach-number similitude*

The preceding discussion indicates that the instability of supersonic mixing layers is quite subtle, and an asymptotic theory can be of great help in clarifying the physics. Although the analysis leading to our asymptotic theory is fairly involved (§§2–6), its main results, in the form of a 'hypersonic' similarity law, are extremely simple.

After performing an affine transformation on the low-speed edge-layer equation, (31*a*), and the associated homogeneous boundary conditions, it is a simple matter to establish

$$\sigma = \mu(1+\hat{c}) = \frac{T_2}{\gamma-1}\mathscr{D}(\kappa T_2), \tag{37a}$$

where the 'universal' (complex) dispersion relation, $\mathscr{D}$, is a function of *one* argument only, say $K = \kappa T_2$. Therefore, the eigenvalue of the *slow* mode (subscript 2) is, via (2*b*),

$$c = c_2 = U_2 + \tfrac{1}{2}\Delta U \frac{T_2}{(\gamma-1)\mu}\mathscr{D}(\kappa T_2), \tag{37b}$$

whose temporal growth rate scales as

$$(kc_1)_2 = \tfrac{1}{2}\Delta U \cos\theta \frac{\kappa T_2}{(\gamma-1)\mu}\mathscr{D}_{\mathrm{I}}(\kappa T_2). \tag{37c}$$

The real and imaginary parts of $\mathscr{D} = \mathscr{D}_{\mathrm{R}} + \mathrm{i}\mathscr{D}_{\mathrm{I}}$ and the universal growth rate curve,

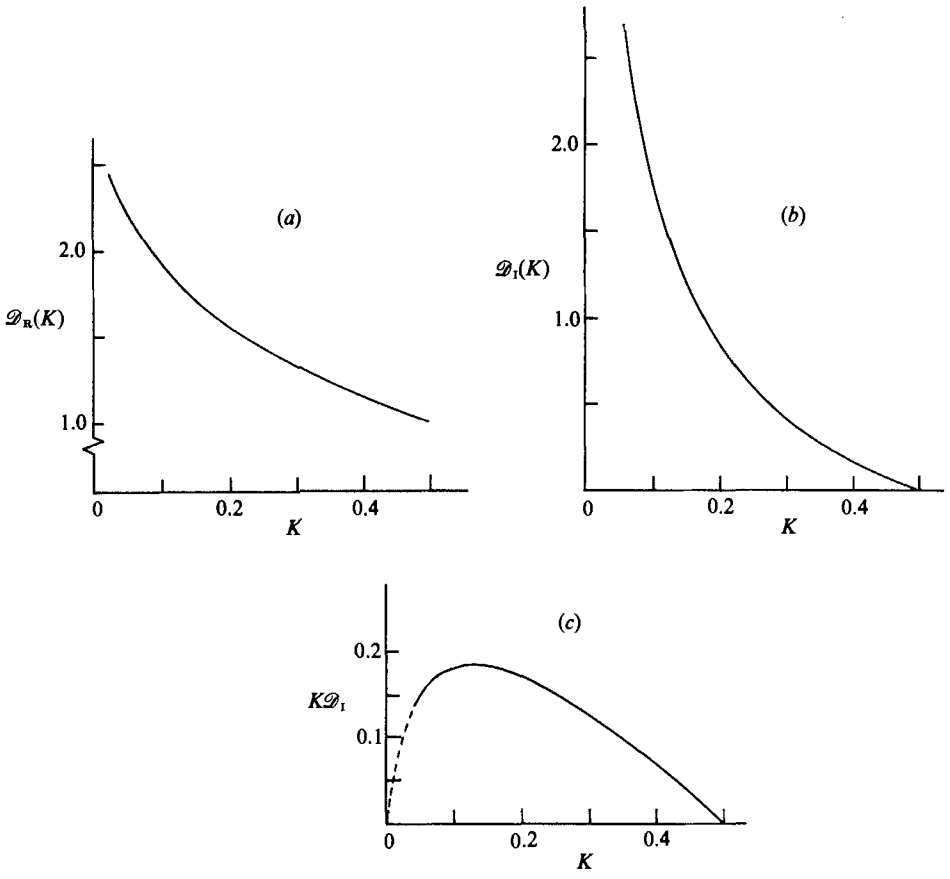

FIGURE 7. Universal dispersion relation: (*a*) real part, (*b*) imaginary part, (*c*) growth rate.

$K\mathscr{D}_I(K)$, are shown in figure 7. These were calculated numerically by solving (31*a*) subject to the homogeneous boundary conditions (35) and (36). For each κ, this problem only possesses a solution for a single complex value of σ, which was determined as part of that solution. We omit the details of our numerical procedure. Note that (31*a*) is, in general, non-singular because σ is, in general complex. We refer to (37*b*, *c*) as our hypersonic similarity law.

A large number of very interesting conclusions may be deduced from this law. Possibly, the most important one is that the eigenvalue of the fast mode (subscript 1) is

$$c_1 - U_1 = -\tfrac{1}{2}\Delta U \frac{1}{(\gamma-1)\mu}\tilde{\mathscr{D}}(\kappa), \tag{38}$$

where the ($\tilde{}$) denotes complex conjugation. The temporal growth rate of the fast mode is also given by (37*c*) with T_2 replaced by unity.

This is because both the fast and the slow modes are localized to the critical layers near $y = \pm\infty$ (or $f = \pm 1$), respectively. In these two narrow regions the shapes of the base flow profiles are identical, except for a scale factor, namely T_2, arising from the Howarth–Dorodnitsyn transformation (i.e. $Y \to y$ as $y \to +\infty$ but $Y \to T_2 y$ as $y \to -\infty$, (3*d*)). The presence of this scale factor in the lower stream explains the rescaling of the wavenumber by this same factor for the slow mode (37*b*).

Slow mode (denoted by subscript 2)

(i) The neutral wavenumber, κ_n, and the wavenumber at the maximum growth rate, κ_m, scale with T_2^{-1}. The factors of proportionality are 0.5 and 0.13 respectively (figure 7*c*);

(ii) the relative speed between the neutral wave and the external stream, U_2, is proportional to $T_2/\mathscr{M}$;

(iii) the maximum growth rate is independent of the temperature ratio but varies as $\mathscr{M}^{-1}$.

Fast mode (denoted by subscript 1)

(i) The characteristics of the fast mode are independent of the temperature ratio, T_2;

(ii) the relative speed between the neutral wave and the external stream, U_1, is proportional to $\mathscr{M}^{-1}$;

(iii) as (iii) for the slow mode.

TABLE 1. Hypersonic similitude

Clearly, at high Mach numbers, the slow and fast modes are related (i.e. they are both governed by the same dispersion relation) and are equally important because they have the same temporal growth rates. This is in contrast to the situation at low supersonic Mach numbers (figure 5) where one of the modes is usually more unstable by a significant amount.

Equation (37*a*) implies that the product $[\sigma(\gamma-1)]$ remains constant at fixed κ and T_2. We therefore expect that in the strict Newtonian limit, $\gamma-1 = O(\mu^{-1})$, σ may become 'large'. This suggests that $|\hat{c}|$ will be substantially different from unity for $\mu \gg 1$ and, consequently, that the phase speed of the resulting instability wave (if one exists) will be supersonic with respect to *both* external streams.

There are two distinct ways of using these similarity laws. The first way is to use (37*b*) and (38), together with figure 7, to predict the eigenvalues, while the second way is to compare the characteristics of the slow and fast modes.

It is possible to draw a large number of conclusions from the hypersonic similarity law and we give a partial list in table 1 (without proof). Note that (37*c*) clearly shows that the most unstable temporal mode is a two-dimensional one and that the important large parameter is $\mathscr{M} = [(\gamma-1)\mu]$ and not simply μ.

The neutral wavenumbers of the slow and fast modes and their respective phase speeds are related by

$$(\kappa_n)_2 = \frac{(\kappa_n)_1}{T_2} \tag{39a}$$

and

$$\frac{(c_R)_2 - U_2}{U_1 - (c_R)_1} = T_2, \tag{39b}$$

or more generally

$$(kc_I)_2(\kappa, T_2) = (kc_I)_1(\kappa T_2) \tag{39c}$$

so that (39*c*) establishes a scaling rule for the temporal growth rate of one of the modes in terms of the other, where $(kc_I)_1(\kappa)$ denotes the growth rate of the fast mode at wavenumber κ (this growth rate is independent of T_2).

Finally

$$(kc_I)_2(\kappa, T_2) = (kc_I)_2(\kappa T_2, 1) \tag{39d}$$

so that the effect of the temperature ratio for the slow mode may be scaled out through the wavenumber.

For the sake of brevity, we do not check here the detailed accuracy of all these facts. However, the overall accuracy of the asymptotic theory can be assessed by examining a particular set of results from Jackson & Grosch (1988) in the light of

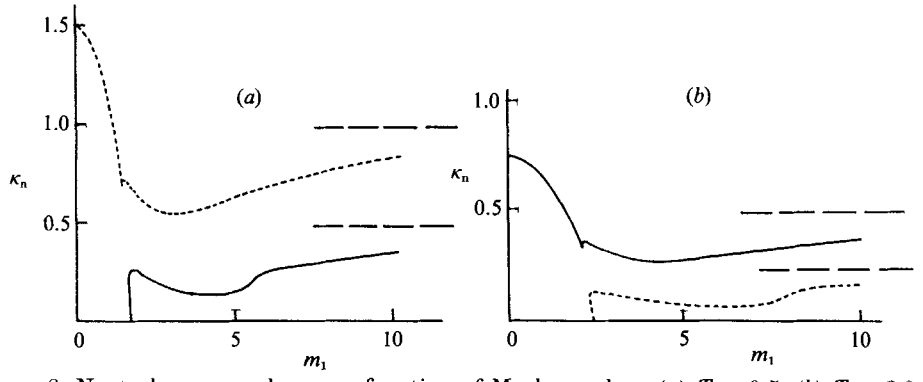

FIGURE 8. Neutral wavenumber as a function of Mach number: (*a*) $T_2 = 0.5$, (*b*) $T_2 = 2.0$ (from Jackson & Grosch 1988 for $\theta = 0$; – – –, high-Mach-number theory); ——, fast mode; ----, slow mode.

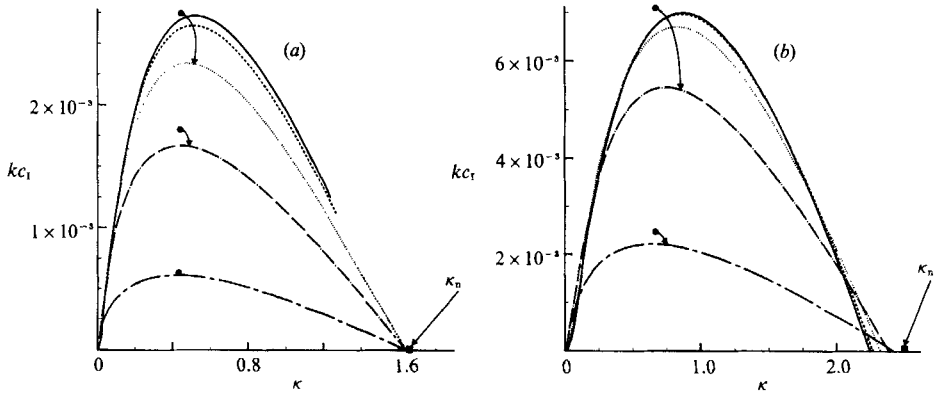

FIGURE 9. Comparison of numerical results and asymptotic theory (●, ■): (*a*) $m_1 = 16$, $T_2 = 0.3$, (*b*) $m_1 = 8$, $T_2 = 0.2$. ——, $\theta = 0$; – – – –, 20°; ....., 40°; —·—·—, 60°; — — — —, 80°.

(39*a*), see figure 8. These results qualitatively confirm the ratio expressed by (39*a*), although the Mach number appears to be too low for a good quantitative comparison. Our asymptotic theory (dashed lines) requires that the other curves should eventually level off.

A more detailed comparison (in the spirit of a prediction) is shown in figure 9. We use figure 7(*c*) and equation (37*c*) to compute the maximum growth rate and the corresponding wavenumber, κ_m. These ordered pairs are indicated by the large dots in the figure, and the arrows show the curves to which the dots belong. The neutral wavenumber of the asymptotic theory is marked by a solid square.

The asymptotic theory clearly works well at very large Mach numbers for (strongly) oblique waves. A decrease in the temperature ratio, T_2, also results in better agreement. In spite of this lack of extensive quantitative agreement at lower Mach numbers, the hypersonic similarity law provides a number of useful rules of thumb and points to the direction for improving the theory.

In an attempt to understand more clearly the limitations of our asymptotic theory, we have carried out an (unpublished) and more involved analysis which shows that the accuracy of our theory hinges on 'transcendentally' small terms. The

scaled eigenvalue, σ, is not truly independent of Mach number, but depends on it through a parameter $\mathscr{P}$ which has the form

$$\mathscr{P} = \exp[-\kappa\mu(\gamma-1)\,\mathscr{V}(\theta)+O(\log\mu)] \tag{40}$$

and, of course, vanishes in the true limit as $\mu\to\infty$. Here $\mathscr{V}(\theta)$ is a monotonically increasing function of the obliqueness angle θ; its value at $\theta = 0$ is 0.24. Through (40) we can clearly see why the asymptotic theory improves as κ or θ increase (see figure 9); we can also see that $\mathscr{P}$ is quite different from zero even when $m_1 = 10$. We chose not to present this more involved analysis because, once the dependence of σ on $\mathscr{P}$ is retained, the hypersonic similarity law is lost (and our main goal is to elucidate the physics rather than to provide a slightly simplified and approximate method for the calculation of the eigenvalues at moderate to high Mach numbers in place of the Rayleigh equation).

7.4. *Spatial instability*

The spatial growth rates for the slow and fast modes may be deduced from the temporal dispersion relations, (37*b*) and (38), by continuing these into complex wavenumber space. For example, for the slow mode, we find

$$\frac{\omega_*}{\cos\theta} = \kappa U_2+\tfrac{1}{2}\Delta U\frac{\kappa T_2}{(\gamma-1)\,\mu}\mathscr{D}(\kappa T_2), \tag{41}$$

where ω_* is the (real) given radian frequency of oscillation of the mode. The solution of (41) for the complex total wavenumber, $\kappa = \kappa(\omega_*)$, may be obtained by successive iteration whenever $|U_2| \gg O(\mu^{-1})$. After substituting

$$\kappa = \kappa^{(0)}+\kappa^{(1)}/\mu+O(\mu^{-2}) \tag{42a}$$

into (41) and expanding in and collecting like powers of μ, we arrive at

$$\kappa^{(0)} = \frac{\omega_*}{U_2\cos\theta} = \text{real} \tag{42b}$$

and

$$\kappa^{(1)} = -\frac{\Delta U}{2U_2}\frac{\kappa^{(0)}T_2}{\gamma-1}\mathscr{D}(\kappa^{(0)}T_2). \tag{42c}$$

The same results apply to the fast mode provided that U_2 is replaced by U_1, $\mathscr{D}$ is replaced by $(-\tilde{\mathscr{D}})$, T_2 is set to unity and κ is replaced by $\tilde{\kappa}$. Clearly (42*b*) establishes a direct proportionality between the lowest-order axial wavenumber, $\kappa^{(0)}\cos\theta$, and the frequency ω_*, and (42*c*) expresses the lowest-order spatial growth rate in terms of the temporal one (which is very reminiscent of the Gaster 1962 transformation).

The key point is that (42*b*, *c*) are valid as long as the relevant external stream velocities are sufficiently different from zero; for the fast mode (say, $U_1 = 1$) the spatial growth rate always decays as μ^{-1}. The last remark also holds at large enough Mach numbers for the slow mode provided that $U_2 \neq 0$; in this case the important frequency which determines the spatial growth rate is $(\omega_* T_2)$ and the maximum growth rate is independent of the temperature ratio.

The situation is *very* different for the slow mode when $U_2 = 0$; roughly speaking, (42*c*) suggests that as $U_2\to 0$ the spatial growth rates may become quite large. First, note from (41) that, for spatial instability the range of unstable frequencies will shrink to zero as μ^{-1}, and whenever the frequency lies in this narrow range, $\kappa T_2 = O(1)$. Thus, the maximum spatial growth rate scales as T_2^{-1}, so that indeed large

growth rates are possible especially when the upper stream is heated. We remind the reader that these conclusions hold for $U_2 = 0$ only, and explain why the slow and fast modes in Jackson & Grosch (1988) behave so differently at large Mach numbers even when $T_2 = 1$.

Our asymptotic theory also reveals that the dominant spatial instability at large Mach numbers is very sensitive to the precise value of $U_2 (\approx 0)$; significant changes in the growth rate can be obtained by changing $(U_2 \mu) = U_2(\frac{1}{2}m_1)^2$ by an $O(1)$ amount. This could have important consequences for experiments (conducted in a finite-size facility).

Finally we briefly explain what happens to the low-speed edge-layer equation when the canonical base velocity profile, f, is given by an arbitrary function. For example, if

$$f \sim -1 + a \exp(-by^2) + \ldots \tag{43}$$

as $y \to -\infty$ (for suitable constants a and b) we can still write $\hat{c} = -1 + \sigma/\mu + \ldots$ and determine σ by a slightly modified version of the low-speed edge-layer equation (31a) provided that κ^2 is allowed to grow as $\log \mu$. Evidently, for this type of velocity profile, the range of unstable wavenumbers weakly increases with Mach number; for the tanh profile this range is finite.

The amplitude of a disturbance must be quite small in order for linearization to be valid in hypersonic flows. Since σ is in general complex, (31a) does not, in general, possess a critical layer for real values of ζ even though the actual growth rate of the instability wave is itself small. We therefore expect nonlinearity to come into play everywhere in the low-speed edge layer once the instability wave amplitude is sufficiently large.

One of us (T.F.B.) is grateful for the hospitality provided by the NASA Lewis Research Center during his sabbatical year when this work was done. Interactions with Dr Lennart Hultgren have been most valuable; we are also deeply indebted to him for sharing with us his knowledge of the computer facilities at NASA Lewis and some of his programs.

Appendix A. Solution in the high-speed edge layer for very oblique waves

When the instability wave is only moderately oblique (so that $\mu \cos^2\theta \gg 1$), the transonic region is separated from the high-speed edge layer by a supersonic region in the main shear layer (figure 1). This case was discussed in §4; the purpose of this Appendix is to describe the solution for very oblique waves for which $\mu \cos^2\theta = O(1)$.

In this case (17a) is rewritten, with the help of (15b),

$$\frac{\mathrm{d}^2\mathscr{R}}{\mathrm{d}\xi^2} + \frac{1}{4\xi^2}\{1 - \kappa^2[1 + (\gamma-1)\xi][(\gamma-1)\xi + \tau^2] + O(\mu^{-1})\}\mathscr{R} = 0, \tag{A 1}$$

where we have put

$$\tau = [1 - \mu \cos^2\theta (1-\hat{c})^2]^{\frac{1}{2}} \tag{A 2}$$

and the branch of the square root is chosen so that the imaginary part is positive when the real part of the argument is negative.

This equation has the solution

$$\mathscr{R} = \xi^{1/2(1+\kappa\tau)} \mathrm{e}^{-1/2\kappa(\gamma-1)\xi}\, {}_1F_1[\tfrac{1}{2}(1+\kappa\tau) + \tfrac{1}{4}\kappa(\tau^2+1); 1+\kappa\tau; \kappa(\gamma-1)\xi], \tag{A 3}$$

where ${}_1F_1$ denotes the confluent hypergeometric function in the usual notation (Abramowitz & Stegun 1970, p. 504). It follows that

$$\mathscr{R} \sim \xi^{1/2(1+\kappa\tau)} \sim \mathrm{e}^{-y(1+\kappa\tau)} \quad \text{as} \quad \xi \to 0 \quad (\text{or } y \to +\infty) \tag{A 4}$$

so that $\mathscr{R}$ satisfies the proper (possibly 'subsonic') boundary condition at $y = +\infty$, and that

$$\mathscr{R} \sim \frac{\Gamma(1+\kappa\tau)\,\xi^{\kappa(\tau^2+1)/4}\,\mathrm{e}^{\kappa(\gamma-1)\xi/2}}{\Gamma[\frac{1}{2}(1+\kappa\tau)+\frac{1}{4}\kappa(\tau^2+1)]} \quad \text{as} \quad \xi\to\infty, \tag{A 5}$$

where Γ denotes the Gamma function. The re-expansion of (8*a*) to (9*b*) with $f_0 = 1$ for constant $\mu\cos^2\theta = O(1)$ yields

$$\mathscr{R} = \exp\left\{\mu\kappa\tfrac{1}{2}(\gamma-1)(1-f)-\tfrac{1}{2}\log[\tfrac{1}{2}(\gamma-1)]+\frac{\kappa}{\gamma-1}\int_0^f J_0(f)\,\mathrm{d}f+\kappa\mu\hat{\phi}_+^{(0)}+\kappa\hat{\phi}_+^{(1)}\right\}, \tag{A 6}$$

where we have put

$$J_0(f) = \frac{\gamma-1}{2(1-f^2)}[\mu\cos^2\theta(f-\hat{c})^2-2T^{(0)}] \tag{A 7}$$

and $T^{(0)} = T^{(0)}(f)$ is defined by (8*e*). In (A 6) $\hat{\phi}_+^{(0)}$ and $\hat{\phi}_+^{(1)}$ are suitable constants of integration which are determined by the asymptotic matching of this special edge-layer solution (A 3) with the WKBJ solution in the main layer (8); this comes about by equating (A 5) to (A 6). The additional details associated with this matching are unimportant for our purposes.

Note that in this case $p \sim \xi^{-\frac{1}{2}}\mathscr{R} \sim \mathrm{e}^{-\kappa\tau y}$ exhibits an oscillatory (or 'supersonic') behaviour as $y\to\infty$ when τ is imaginary and that it grows exponentially as $(1-f) = \xi/\mu\to\infty$ (i.e. (A 6)). In other words, the edge layer may convert the primarily exponential solution (which exists in the main layer when $f_0 = 1$) into a primarily oscillatory solution, which exists in the fast external stream. In this sense, the edge layer is reminiscent of the turning-point region of a classical WKBJ problem. Note that the edge layer is needed even when τ is (nearly) real. We emphasize that these remarks and the derivations that follow (A 1) are valid when $f_0 = 1$ (specifically $\theta \approx \frac{1}{2}\pi$; see (11)). In this case the turning point has moved into the high-speed edge layer and the supersonic region in the main part of the shear layer has disappeared.

Appendix B. A particular solution to the inhomogeneous Airy equation

A straightforward application of the variation of parameters shows that

$$\mathscr{R}_*^{(\frac{1}{3})} = H_1(\eta)\,\mathrm{Ai}\,(\eta A^{\frac{1}{3}})+H_2(\eta)\,\mathrm{Bi}\,(\eta A^{\frac{1}{3}}), \tag{B 1}$$

where $\mathscr{R}_*^{(\frac{1}{3})}$ is a particular solution of (23*a*) at $O(\mu^{-\frac{1}{3}})$ and

$$H_1(\eta) = \frac{\pi B}{A^{\frac{1}{3}}}\left\{\alpha^{(0)}\int_0^\eta \mathrm{Ai}\,(\hat{\eta})\,\mathrm{Bi}\,(\hat{\eta})\,\mathrm{d}\eta'+\beta^{(0)}\int_0^\eta \mathrm{Bi}^2\,(\hat{\eta})\,\mathrm{d}\eta'\right\}, \tag{B 2}$$

$$H_2(\eta) = -\frac{\pi B}{A^{\frac{1}{3}}}\left\{\alpha^{(0)}\int_\infty^\eta \mathrm{Ai}^2\,(\hat{\eta})\,\mathrm{d}\eta'+\beta^{(0)}\int_0^\eta \mathrm{Ai}\,(\hat{\eta})\,\mathrm{Bi}\,(\hat{\eta})\,\mathrm{d}\eta'\right\}, \tag{B 3}$$

where $\hat{\eta} = \eta' A^{\frac{1}{3}}$. The notation is borrowed from the main part of the paper. For $\eta\to+\infty$

$$\int_0^\eta \mathrm{Ai}\,(\hat{\eta})\,\mathrm{Bi}\,(\hat{\eta})\,\mathrm{d}\eta' = \frac{\eta^{\frac{1}{2}}}{\pi A^{\frac{1}{6}}}+O(1), \tag{B 4a}$$

$$\int_\infty^\eta \mathrm{Ai}^2\,(\hat{\eta})\,\mathrm{d}\eta' = O(\eta^{-1}) \tag{B 4b}$$

and $$\int_0^{\eta} \mathrm{Bi}^2(\hat{\eta})\,\mathrm{d}\eta' = O[\eta^{-1}\exp(+\tfrac{4}{3}\eta^{\frac{3}{2}}A^{\frac{1}{2}})]. \tag{B 4c}$$

Note that in (B 4c) the argument of the exponential is positive and large; in spite of this we do not need to consider it in our final expression because of the presence of even larger terms. On the other hand, as $\eta \to -\infty$

$$\int_0^{\eta} \mathrm{Ai}(\hat{\eta})\,\mathrm{Bi}(\hat{\eta})\,\mathrm{d}\eta' = O(1), \tag{B 5a}$$

$$\int_{\infty}^{\eta} \mathrm{Ai}^2(\hat{\eta})\,\mathrm{d}\eta' = -\frac{(-\eta)^{\frac{1}{2}}}{\pi A^{\frac{1}{6}}} + O(1), \tag{B 5b}$$

$$\int_0^{\eta} \mathrm{Bi}^2(\hat{\eta})\,\mathrm{d}\eta' = -\frac{(-\eta)^{\frac{1}{2}}}{\pi A^{\frac{1}{6}}} + O(1). \tag{B 5c}$$

After combining the above equations we find

$$\mathscr{R}_*^{(\frac{1}{3})} = -B\frac{\dfrac{\eta^{\frac{1}{2}}}{A^{\frac{1}{2}}} + O(1)}{\pi^{\frac{1}{2}}A^{\frac{1}{12}}\eta^{\frac{1}{4}}}\beta^{(0)}\exp(+\tfrac{2}{3}\eta^{\frac{3}{2}}A^{\frac{1}{2}}) \quad \text{as} \quad \eta \to +\infty, \tag{B 6a}$$

where we have tacitly assumed that $\beta^{(0)} \neq 0$, and

$$\mathscr{R}_*^{(\frac{1}{3})} = -B\frac{\dfrac{(-\eta)^{\frac{1}{2}}}{A^{\frac{1}{2}}} + O(1)}{\pi^{\frac{1}{2}}A^{\frac{1}{12}}(-\eta)^{\frac{1}{4}}}\{\beta^{(0)}\sin[\tfrac{2}{3}(-\eta)^{\frac{3}{2}}A^{\frac{1}{2}} + \tfrac{1}{4}\pi] - \alpha^{(0)}\cos[\tfrac{2}{3}(-\eta)^{\frac{3}{2}}A^{\frac{1}{2}} + \tfrac{1}{4}\pi]\} \quad \text{as} \quad \eta \to -\infty. \tag{B 6b}$$

Appendix C. Behaviour of the WKBJ solution near the low-speed edge layer

The WKBJ phases in the subsonic region, the integrals in (9a) and (10a), rewritten in terms of the low-speed edge-layer variable ζ, expanded in μ and truncated after the one-term edge-layer expansion, are

$$\mu\int_f^{f_0} g(f)\,\mathrm{d}f \to [\tfrac{1}{2}(\gamma-1)]^{\frac{1}{2}}\int_0^{1+f_0}\frac{\mathrm{d}x}{(2-x)^{\frac{1}{2}}}\left\{\mu h^{\frac{1}{2}} + \frac{\sigma\cos^2\theta}{h^{\frac{1}{2}}}\right\} - \tfrac{1}{2}(\gamma-1)\zeta, \tag{C 1a}$$

where $$h = h(x) = \tfrac{1}{2}(\gamma-1)(2-x) - x\cos^2\theta \tag{C 1b}$$

and

$$\int_f^{f_0}\frac{J(f)}{g(f)}\,\mathrm{d}f \to T_2\left(\log\zeta - \log\mu - \log\frac{8\nu}{1+\nu}\right) + \int_0^{1+f_0}\frac{T_*\dfrac{x\cos^2\theta - (\gamma-1)(2-x)}{[\frac{1}{2}(\gamma-1)]^{\frac{1}{2}}(2-x)^{\frac{3}{2}}} + F_*}{xh^{\frac{1}{2}}}\,\mathrm{d}x, \tag{C 2a}$$

where $$T_* = T_*(x) = T_2 + \tfrac{1}{2}(1-T_2)\,x, \tag{C 2b}$$

$$F_* = \text{const.} = (\gamma-1)^{\frac{1}{2}}T_2, \tag{C 2c}$$

and ν is defined by (11b). After finding the behaviour of the WKBJ solution, (8) and

(9), near the low-speed edge layer with the help of the above equations, and equating this quantity to (36), $\epsilon_{-}(\mu) = \text{const.}$ is readily determined.

REFERENCES

ABRAMOWITZ, M. & STEGUN, I. A. 1970 *Handbook of Mathematical Functions*. Dover.

BENNEY, D. J. & BERGERON, R. F. 1969 A new class of nonlinear waves in parallel flows. *Stud. Appl. Maths* **48**, 181–204.

BETCHOV, R. & CRIMINALE, W. O. 1967 *Stability of Parallel Flow*. Academic.

BLUMEN, W. 1970 Shear layer instability of an inviscid compressible fluid. *J. Fluid Mech.* **40**, 769–781.

BLUMEN, W., DRAZIN, P. G. & BILLINGS, D. F. 1975 Shear layer instability of an inviscid compressible fluid. Part 2. *J. Fluid Mech.* **71**, 305–316.

BODONYI, R. J., SMITH, F. T. & GAJJAR, J. 1983 Amplitude-dependent stability of boundary-layer flow with a strongly nonlinear critical layer. *IMA J. Appl. Maths* **30**, 1–19.

COWLEY, S. J. & HALL, P. 1990 On the instability of hypersonic flow past a wedge. *J. Fluid Mech.* **214**, 17–42.

DRAZIN, P. G. & REID, W. H. 1981 *Hydrodynamic Stability*. Cambridge University Press.

GASTER, M. 1962 A note on the relation between temporally-increasing and spatially-increasing disturbances in hydrodynamic stability. *J. Fluid Mech.* **14**, 222–224.

GROPENGIESSER, H. 1969 Study on the stability of boundary layers in compressible fluids. *NASA TT* F-12, p. 786. (Transl. of DLR-FB-69-25.)

HAYES, W. D. & PROBSTEIN, R. F. 1966 *Hypersonic Flow Theory*. Academic.

JACKSON, T. L. & GROSCH, C. E. 1988 Spatial stability of a compressible mixing layer. *NASA CR*-181671.

KEMBLE, E. C. 1935 A contribution to the theory of the B.W.K. method. *Phys. Rev.* **48**, 549–561.

KUMAR, A., BUSHNELL, D. M. & HUSSAINI, M. Y. 1987 A mixing augmentation technique for hypervelocity scramjets. *AIAA Paper* 87-1882.

LEES, L. & LIN, C. C. 1946 Investigation of the stability of the laminar boundary layer in a compressible fluid. *NACA TN*-1115.

LESSEN, M., FOX, J. A. & ZIEN, H. M. 1965 On the inviscid stability of the laminar mixing of two parallel streams of a compressible fluid. *J. Fluid Mech.* **23**, 355–367.

MILES, J. W. 1958 On the disturbed motion of a plane vortex sheet. *J. Fluid Mech.* **4**, 538–552.

MOORE, F. K. (ed.) 1964 *Theory of Laminar Flows*. Princeton University Press.

NAYFEH, A. H. 1973 *Perturbation Methods*. Wiley.

PAPAMOSCHOU, D. 1986 Experimental investigation of heterogeneous compressible shear layers. Ph.D. thesis, Caltech.

SCHLICHTING, H. 1966 *Boundary-Layer Theory*. McGraw-Hill.

SMITH, F. T. 1987 On boundary-layer thickening in transition, and vorticity slugs in internal flows. *United Technology Research Center Rep.* UTRC 87-43.

TAM, C. K. W. & HU, F. Q. 1988 Instabilities of supersonic mixing layers inside a rectangular channel. *Proc. 1st Natl Fluid Dynamics Conf.*, Part 2, pp. 1073–1086.

VAN DYKE, M. 1975 *Perturbation Methods in Fluid Mechanics*. Parabolic.